Nuclear Instruments and Methods in Physics Research B 283 (2012) 63–70

Contents lists available at SciVerse ScienceDirect

Nuclear Instruments and Methods in Physics Research B

journal homepage: www.elsevier.com/locate/nimb

Theoretical study of the double ionization of the He isoelectronic sequence by protons and antiprotons

S.D. López [a,*], C.R. Garibotti [a], S. Otranto [b]

[a] CONICET and Centro Atómico Bariloche, Av. Bustillo Km 9.4, 8400 S.C. de Bariloche, Argentina
[b] IFISUR and Departamento de Física, Universidad Nacional del Sur, 8000 Bahía Blanca, Argentina

ARTICLE INFO

Article history:
Received 17 January 2012
Received in revised form 20 April 2012
Available online 30 April 2012

Keywords:
Double ionization
Fully differential cross sections
Isoelectronic sequence of He

ABSTRACT

We evaluate the fully differential cross sections (FDCS) for the double ionization of the He-isoelectronic sequence by proton and antiproton impact. We use a distorted wave model recently introduced by the authors based on static and dynamically screened charges for the final continuum state. We identify three main collision mechanisms, which we denote as: back-to-back, recoil and binary emissions. We discuss the relative relevance in the FDCS of these mechanisms as the electron emission energies and nuclear charges are varied. We study the variation of the electronic angular distributions according to well established scaling rules for the electron momenta and energies. The dependence of the FDCS on the projectile charge sign is analyzed and found to become more relevant for increasing nuclear charges of the target.

1. Introduction

In recent years, collision processes involving more than one active electron (multiple capture or ionization, transfer ionization processes), have been found relevant in areas like astrophysics or biological and medical sciences [1–4]. There, multielectronic targets in gas phase (atoms and molecules) and (eventually) highly charged projectiles provide an ideal environment for these processes to take place, requiring for their study an appropriate experimental and theoretical knowledge not usually at hand. As a particular case, the double ionization of He problem has been addressed starting in the 1980s, when the first measurements of the total cross section (TCS) were made [5,6]. The theoretical counterparts in those days were provided by (i) perturbative methods based on two-step mechanisms (i.e. they considered the projectile colliding two times with the atom ejecting one electron at a time) further improved in subsequent years [7–12]; (ii) Exhaustive numerical efforts based on the forced impulse method, using a large number of two-electron pseudostates for the ionization continuum [13] or (iii) classical descriptions like the one provided by the classical trajectory Monte Carlo (CTMC) method [14].

The development of the reaction microscopy technique by the mid 1990s, usually termed cold target recoil ion momentum spectroscopy (COLTRIMS), gave potential accessibility to higher order differential cross sections for atomic and molecular collisions involving photon, electron and ion impact. In 2003, Fischer [15] presented fully differential cross sections (FDCS) for double ionization of He by proton impact at 6 MeV impact energy. In that work the results were compared with their electron impact counterpart concluding that the several differences in the structure of the FDCS are consequence of the difference in the charge sign of the projectile. These authors also presented doubly differential cross sections (DDCS) for the same process, which resulted from the integration of the FDCS over the projectile momentum transfers involved.

Theoretical studies motivated by the COLTRIMS pioneering work, have mostly been devoted to explain the origin of the structures in the FDCS (or DDCS), usually represented in terms of contour plots as a function of the coplanar emission angles (θ_1 and θ_2) of both electrons [16–18]. Since only low energy electrons are detected to avoid prohibitive extraction fields, the agreement between the experimental and theoretical spots has been pursued, rather than a more exhaustive analysis based in the FDCS magnitudes. Furthermore, some of those works apply statistical integration techniques to simulate different successive collisions between the particles involved, but do not lead to differences at the fully differential level for projectiles having different charge sign. Other numerically intensive methods give very good agreement with the experimental DDCS from Fischer [19,20] and the antiproton impact TCS from CERN [20].

In a recent work [21], the projectile-charge-sign dependence of the FDCS has been theoretically studied by means of a continuum distorted wave model which, through a set of effective charges for the electrons-target nucleus interactions, incorporates the influence of the receding projectile in the two-electron-continuum atomic subsystem. This study suggested that at impact energies of about 6 MeV/amu the proton–antiproton differences at the fully differential level were negligible for the collision geometries

* Corresponding author.
E-mail address: sebastian.lopez@cab.cnea.gov.ar (S.D. López).

0168-583X/$ - see front matter © 2012 Elsevier B.V. All rights reserved.
http://dx.doi.org/10.1016/j.nimb.2012.04.018

explored, fact that was ascribed to the intermediate-to-low range of momentum transfers explored. Furthermore, within the distorted wave model, it has been shown that FDCS obtained by models explicitly including the final state interaction among the emitted electrons at the wavefunction level ($\Psi(\mathbf{r}_1,\mathbf{r}_2,\mathbf{r}_{12})$), differ by more than one order of magnitude with those which are solely based on correlation factors ($\Psi(\mathbf{r}_1,\mathbf{r}_2)\times C(k_{12})$) [8–11,22]. Only through the systematic exploration of doubly ionization processes for different collision geometries it will be possible to determine at which extent the usually recalled simpler models can be considered reliable in terms of the absolute magnitudes predicted.

The purpose of this work is threefold. In the first place, we analyze "three classical pictures" for the emission of two electrons with equal energies. The identification of these collision mechanisms allow a more elaborate interpretation of the FDCS in terms of contour plots. We explore the influence of the atomic nucleus charge in the electronic double emission. For this purpose we use angular correlated variational wave functions for two electron ions proposed by Otranto et al. in the initial state [23], and for the final state we employ Three Body Coulomb (3C) based models [21,24–27]. In second place, we consider the He-isoelectronic sequence discussing the influence of the relative weight of the electron–electron and the electron–nuclear target interactions and seek for possible signatures that can be traced at the fully differential level. In third place, we analyze the scaling properties of the FDCS. In previous works, scalings for the FDCS for different target nucleus charges were calculated for different processes as atomic photo-double-ionization (PDI) of two electron ions [28,29], single ionization of atoms by electron impact [30,31] or double ionization of the isoelectronic series of He by electron impact [32,33]. In this work we contribute to the subject by showing the substantial differences that arise in the angular distributions when low nuclear charges are considered in a scaled regime.

Finally we consider the projectile charge sign influence in the electronic distributions for double ionization of the lower ions in the isoelectronic series of He via the model proposed by Gasaneo and Otranto (GO) used in [21,34] similar to that of Jetzke and Faisal [35].

Atomic units are used throughout this work unless otherwise stated.

2. Theory

We consider the double ionization of the isoelectronic series of He up to $Z_T=5$ by bare ions impact with initial (final) momentum $\mathbf{K_i}$ ($\mathbf{K_f}$) of the projectile relative to the atomic center of mass. We denote with $\mathbf{k}_1$ and $\mathbf{k}_2$ to the final momenta of the electrons relative to the target. Since intermediate to high impact energies are explored, we only consider a first order interaction between the projectile and the target atom. As a result, in the initial state we represent the projectile by means of a plane wave. For the projetile final state, we make either use of a Kummer function or a plane wave depending on whether the postcollisional interaction of the receding projectile is considered or not. Within this context, the FDCS can be written as:

$$\frac{d\sigma}{d\mathbf{k}_1 d\mathbf{k}_2 d\mathbf{Q}_\perp}=\frac{(2\pi)^4}{V^2}\left|T_{fi}\right|^2. \tag{1}$$

Here, V is the impact speed, $\mathbf{Q}_\perp$ is the perpendicular component to the beam direction of the momentum transfer defined as: $\mathbf{Q}=\mathbf{K_i}-\mathbf{K_f}$. The first order transition matrix T_{fi} in a distorted wave formalism is given by

$$T_{fi}=\left\langle \chi_f^-\middle| W_i\middle|\chi_i^+\right\rangle, \tag{2}$$

where the operator W_i represents the unsolved part of the initial Hamiltonian:

$$W_i=\frac{Z_P Z_T}{R}-\frac{Z_P}{|\mathbf{R}-\mathbf{r}_1|}-\frac{Z_P}{|\mathbf{R}-\mathbf{r}_2|}. \tag{3}$$

The initial state used in this work is given by:

$$\chi_i^+=\frac{1}{(2\pi)^{3/2}}e^{i\mathbf{K_i}\cdot\mathbf{R}}\Psi_i^+(\mathbf{r}_1,\mathbf{r}_2), \tag{4}$$

where the atomic initial ground state (GS2) has the shape:

$$\Psi_i^+(\mathbf{r}_1,\mathbf{r}_2)=N_i\left(e^{-ar_1-br_2}+e^{-br_1-ar_2}\right)\left(e^{-z_c r_{12}}+C_0 e^{-\lambda r_{12}}\right). \tag{5}$$

The values of the different constants are those of table I of the reference [23]. The coordinates $\mathbf{r}_1$ and $\mathbf{r}_2$ are the electronic positions with respect to the target nucleus, and $\mathbf{r}_{12}=\mathbf{r}_1-\mathbf{r}_2$ is the relative position between the electrons.

For the final state, three options are considered and the discussion will be centered in the effects produced by these models in the electronic distributions.

(i) The three-body Coulomb model (3C) [24,25]

In this case the final wave function for the system is:

$$\chi_f^-=\frac{1}{(2\pi)^{3/2}}e^{i\mathbf{K_f}\cdot\mathbf{R}}\Psi_f^-(\mathbf{r}_1,\mathbf{r}_2), \tag{6}$$

with the electrons continuum described by:

$$\Psi_f^-(\mathbf{r}_1,\mathbf{r}_2)=\frac{1}{(2\pi)^3}\times\frac{(1+P_{12})}{\sqrt{2}}\left[e^{i(\mathbf{k}_1\cdot\mathbf{r}_1+\mathbf{k}_2\cdot\mathbf{r}_2)}D_{\mathbf{k}_1}(\eta_1,\mathbf{r}_1)D_{\mathbf{k}_2}(\eta_2,\mathbf{r}_2)D_{\mathbf{k}_{12}}(\eta_{12},\mathbf{r}_{12})\right]. \tag{7}$$

Here $\eta_{1,2}=-Z_T/k_{1,2}$, $\mathbf{k}_{12}=\frac{1}{2}(\mathbf{k}_1-\mathbf{k}_2)$, $\eta_{12}=1/2k_{12}$ and P_{12} is the permutation operator. The Coulomb distortion has the well known shape:

$$D_{\mathbf{k}}(\eta,\mathbf{r})=\Gamma(1-i\eta)e^{-\frac{\eta\pi}{2}}{}_1F_1[i\eta,1,-i(kr+\mathbf{k}\cdot\mathbf{r})] \tag{8}$$

This model overestimates the repulsion between the electrons when the emission energy of them decreases, the cross sections in this case presents an exponential decreasing behavior in contrast with the Wannier theories that predict a power law dependence [36].

(ii) The dynamical screening three-body Coulomb model (DS3C)

This model, conceptually proposed by Berakdar and Briggs in 1994 [26] for equal energy electrons, represents an improvement over the 3C model. By means of dynamical charges that allow the three particles to exchange momentum, they attempted to incorporate the non orthogonal kinetic energy neglected in the 3C three body Hamiltonian. The dynamical charges of this model, as later on presented by Berakdar for electrons with arbitrary energies are [27]:

$$Z^{DS}_{e_1-He^{+}}=-Z_T+Z_{eff_1}(k_1,k_2,k_{12}) \tag{9}$$

$$Z^{DS}_{e_2-He^{+}}=-Z_T+Z_{eff_2}(k_1,k_2,k_{12}) \tag{10}$$

$$Z^{DS}_{e_1-e_2}=1-Z_{eff_{12}}(k_1,k_2,k_{12}) \tag{11}$$

with

$$Z_{eff_1}(k_1,k_2,k_{12})=\left(\frac{3+\cos^2 4\alpha_1}{4}\frac{k_1}{k_1+k_2}\right)^2\frac{k_{12}}{k_1+k_2} \tag{12}$$

$$Z_{eff_2}(k_1,k_2,k_{12})=\left(\frac{3+\cos^2 4\alpha_2}{4}\frac{k_2}{k_1+k_2}\right)^2\frac{k_{12}}{k_1+k_2} \tag{13}$$

$$Z_{eff_{12}}(k_1,k_2,k_{12})=\left(\frac{3+\cos^2 4\alpha_1}{4}\frac{k_{12}}{k_1+k_2}\right)^2\frac{k_1}{k_1+k_2}+\left(\frac{3+\cos^2 4\alpha_2}{4}\frac{k_{12}}{k_1+k_2}\right)^2\frac{k_2}{k_1+k_2}, \tag{14}$$

and the coefficients α_1 and α_2

$$\alpha_1 = \arccos\frac{k_2}{\sqrt{k_1^2+k_2^2}} \tag{15}$$

$$\alpha_2 = \arccos\frac{k_1}{\sqrt{k_1^2+k_2^2}}. \tag{16}$$

This model was employed with some success in (e,2e) and (e,3e) studies with low energy emission [26,27,37].

(iii) DS3C GO model

To introduce the postcollisional interaction of the receding projectile over the atomic sub-system, we introduce the Jetzke-Faisal first order multiple scattering model [35] as adapted for the present problem by López et al. [21]. Its implementation results in the nuclear–nuclear interaction being explicitly included in the final state through a Coulomb wave function:

$$\chi_f^- = \frac{1}{(2\pi)^{3/2}} e^{i\mathbf{K_f}\cdot\mathbf{R}} D_{\mathbf{k_f}}(\eta_{NN},\mathbf{R})\Psi_f^-, \tag{17}$$

and the following set of effective charges for the electrons–target interactions and the nuclear–nuclear interaction:

$$Z^{GO}_{e_1-He} = Z^{DS}_{e_1-He^+} + Z_P\frac{\mathbf{k}_{1P}.\mathbf{k}_1}{k_{1P}^3}k_1 \tag{18}$$

$$Z^{GO}_{e_2-He} = Z^{DS}_{e_2-He^+} + Z_P\frac{\mathbf{k}_{2P}.\mathbf{k}_2}{k_{2P}^3}k_2 \tag{19}$$

$$Z^{GO}_{e_1-e_2} = Z^{DS}_{e_1-e_2} \tag{20}$$

$$Z_{PT} = Z_P\left(Z_T + \frac{\mathbf{k}_{1P}.\mathbf{V}}{k_{1P}^3}V + \frac{\mathbf{k}_{2P}.\mathbf{V}}{k_{2P}^3}V\right). \tag{21}$$

Here, Z_P is the projectile charge, $\boldsymbol{V}$ is the final projectile velocity and $\mathbf{k_{iP}}$ the ith electron momentum relative to the projectile.

The Gram-Schmidt procedure has been used in all cases in the forthcoming analysis, for orthogonalization of the final to initial atomic state. As a result, the perturbation element Z_PZ_T/R does not provide any contribution to the transition matrix element.

3. Fully differential cross sections as contour plots

The FDCS for double ionization of He by proton impact have been presented by using a contour plot representation as a function of the coplanar emission angles (θ_1 and θ_2) of both electrons. All the reaction fragments remain in the collision plane defined by the initial and final projectile momentum vectors. This representation was already used by Dorn et al. [38] in their (e,3e) studies and differs from that used by the group of Lahmam–Benanni [39], which used the typical angular distributions common to the (e,2e) field. In fact, the latter can be simply seen as the profile of selected cuts of the former.

Provided that so far only equal energy results have been measured in the ion-atom context [15], in the following we discuss three collision mechanisms that can be associated to classical pictures which allow a fast visualization of the information provided by the different "spots" in the contour plot. Terms like "binary peak" and "recoil peak" are well known to the single ionization community and provide a fast visual guide, based on classical terms, on the relative importance of the different interactions (projectile–electron, electron–target nucleus, projectile–target nucleus) acting through a collision process. However, it is also well known that these pictures strictly apply to well determined emission geometries [40] and as such should be taken with caution.

In the contour plot representation, the momentum transfer direction is fixed and the electrons momenta rotate with angles θ_1 and θ_2 in the collision plane. Thus, following the momentum conservation law: $\mathbf{Q} = \mathbf{k}_1 + \mathbf{k}_2 + \mathbf{R}$, we observe that as $\mathbf{k}_1$ and $\mathbf{k}_2$ change, an expression for the recoil momentum can be obtained. From the evaluation of different FDCS for double electron emission under equal energy regime, we clearly distinguish three main structures in the distributions which can be characterized by the particular values of the momentum $\boldsymbol{R}$ acquired by the recoiling nucleus once the collision has taken place:

- "*back-to-back emission*": In this case, both electrons are ejected in opposite directions ($\mathbf{k}_1 + \mathbf{k}_2 \approx 0$) with $\mathbf{R} \approx \mathbf{Q}$. This structure can be explained in terms of successive classical collisions considering that the projectile hits one electron and this electron hits the nucleus going backwards with $\mathbf{k}_1 = -\mathbf{Q}$. The nucleus then recoils with $\mathbf{R} \approx 2\mathbf{Q}$ and hits the other electron, which acquires a momentum $\mathbf{k}_2 = \mathbf{Q}$ (see Fig. 1a).

- "*Recoil emission*": In this case (Fig. 1b), the total momentum of the electrons has the same magnitude but is opposite to the momentum transfer ($\mathbf{k}_1 + \mathbf{k}_2 \approx -\mathbf{Q}$). This configuration implies that the nucleus recoils with $\mathbf{R} \approx 2\mathbf{Q}$. From a classical point of view it can be explained as follows: the projectile hits one electron which is scattered backward by the nucleus and, this electron knocks the other one before leaving the atom. The electrons leave the reaction zone with a relative angle equal to 90° . As we are dealing with quantum systems, and the target nucleus is present, the correct statement is that relative angles are wider than 90° and that is the reason for which we did not draw $\mathbf{k}_1$ and $\mathbf{k}_2$ strictly orthogonal.

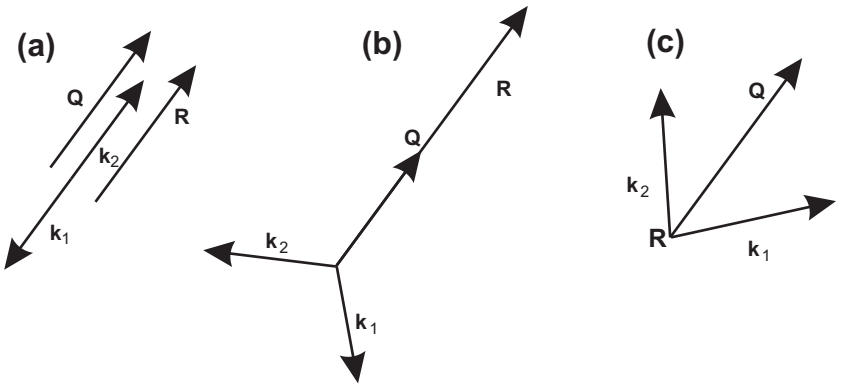

Fig. 1. Vectorial schemes for the four body momentum sharing in the final state. The schemes are those corresponding to the classical collisions mechanisms, as described in text. These schemes are denoted as (a): "Back to Back emission", (b): "Recoil emission" and (c): "Binary emission".

- "*Binary emission*": In this situation (Fig. 1c), the total electronic momentum is similar to the momentum transfer ($\mathbf{k}_1 + \mathbf{k}_2 \approx \mathbf{Q}$) and the recoil ion is mainly an spectator during the collision ($\mathbf{R} \approx 0$). The projectile transfers the momentum to one electron which then hits the second one, and both are emitted in quasi-orthogonal directions while the nucleus remains almost still. This mechanism is similar to the binary collision in single ionization.

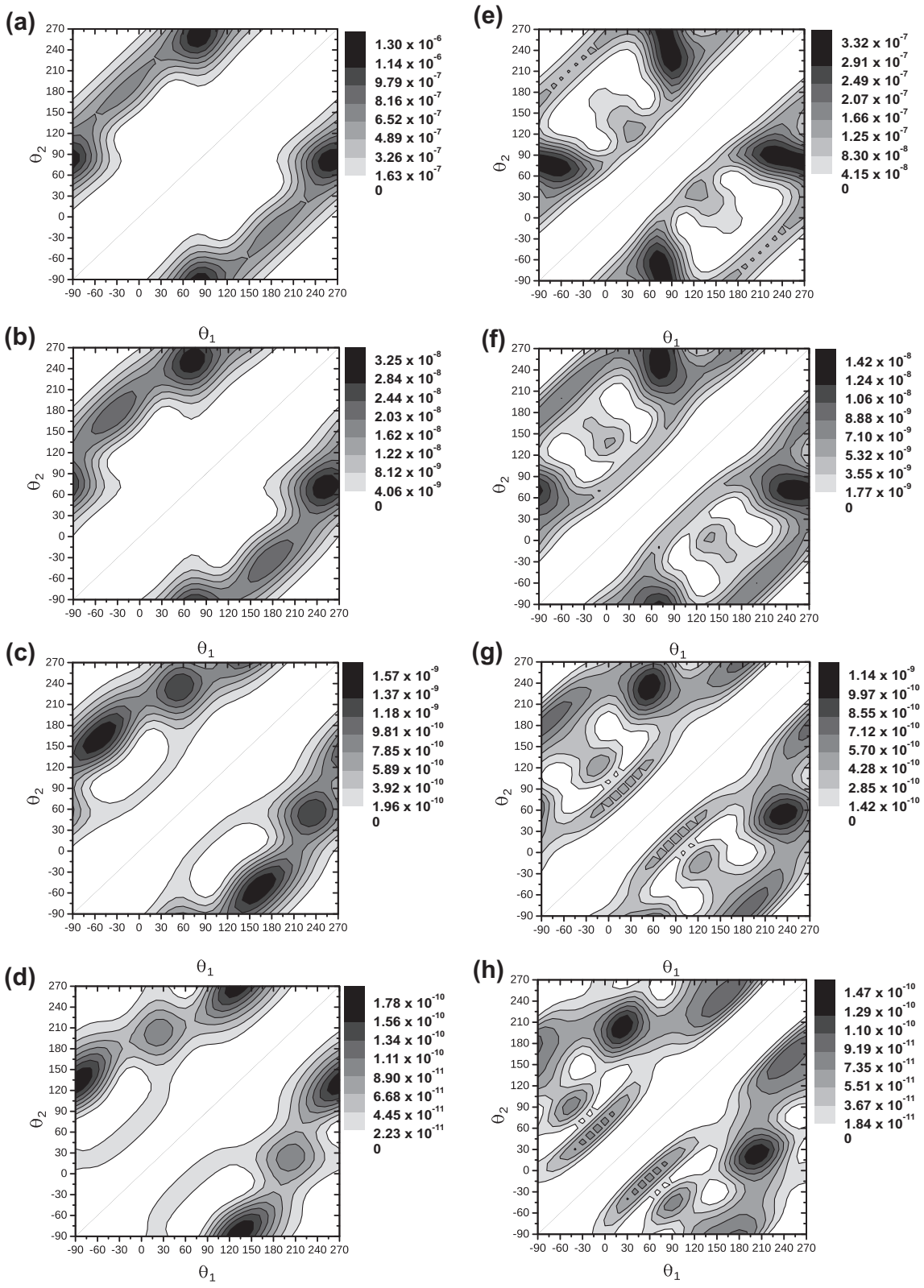

Fig. 2. FDCS (in a.u.) for two ejected electrons with $E_1 = E_2 = 10$ eV in 6 MeV proton impact collisions. The θ_1 and θ_2 angles are measured counter clockwise from the incident beam direction. The momentum transfer is $Q = 1.6$ a.u. The contour plots (a)–(d) correspond to the GS2 initial wave functions with 3C final waves, (e)–(h) to the GS2 initial waves with DS3C final states. The (a) and (e) plots corresponds to He target, (b) and (f) to Li^+, (c) and (g) to Be^{2+}, and (d) and (h) to B^{3+}.

We now present our results for FDCS for the double ionization of atoms in the He isoelectronic sequence. The different structures are discussed in terms of the here recalled mechanisms.

4. Results

4.1. Double ionization FDCS for He and He-like ions

In first place we study the dependence of the FDCS on an increasing target nuclear charge. We consider the double ionization of He, Li^+, Be^{2+}, B^{3+} for proton impact at 6 MeV. The momentum transfer magnitude Q is 1.6 a.u. and the two electrons are emitted with the same energy of 10 eV. In Fig. 2a–d we show the FDCS within the 3C final atomic state model. In the second column, Fig. 2e–h, we present similar results obtained with the DS3C model. Among the general results observed, the first important feature that we note is the symmetry with respect to the diagonal $\theta_1 = \theta_2$ as a consequence that the electrons are indistinguishable. Second, the FDCS obtained with the 3C model have larger magnitudes than those obtained with the DS3C model. This feature could sound strange at first sight if one considers that the DS3C model was built to improve the exponential decreasing behavior of the 3C model at low emission energies. However, from photo-double-ionization studies on He target [41], it is well known that in the equal energy regime the 3C wavefunction provides FDCS which tend to overestimate the cross sections in magnitude for excess energies above 10 eV for each electron. It could be possible that the DS3C not only improves the threshold region description compared to the pure 3C model, but also tends to correct the cross section magnitudes as the emission energy increases. Finally, the FDCS magnitude decreases with increasing nuclear charge as expected due to the increasing binding energy. On the other hand, we note that both models lead to different relative magnitudes for the observed structures.

We now perform a closer inspection of the structures seen in Fig. 2. For He target (Fig. 2a and e) the dynamical configuration selected leaves the **Q** direction at $\theta_Q = 81.5^\circ$ in the collision plane. The principal structure that we note is that corresponding to the "back-to-back emission" placed around $\theta_1 \approx 81^\circ$ and $\theta_2 \approx 260^\circ$. For the 3C model, we observe other large emission region for a relative angle θ_{12} of about 160°, which can be produced by the mediation of the recoil ion. There, the magnitude of the FDCS is about half of that given by the "back-to-back emission" and results from the overestimation of the inter-electronic repulsion in the 3C model. Furthermore, in this model the strong repulsion between the electrons tends to push them away in opposite directions and the binary emission is negligible. In the DS3C model results, on the other hand, we observe a more complex pattern: we find a non-vanishing probability of double electronic emission for smaller θ_{12} values compared to the 3C results. This could be due to the fact that this model allows for momentum exchange between the three particles, diminishing the relevance of the inter-electronic repulsion. The main feature in the DS3C spectra, in concordance with the 3C results, is the "back-to-back emission", that duplicates the other structures in magnitude. The "recoil emission" is a stripe centered at $\left(\theta_1 \approx 210^\circ, \theta_2 \approx -40^\circ\right)$ with θ_{12} about 110°, while the "binary emission" at $\left(40^\circ, 120^\circ\right)$, has its maximum for $\theta_{12} = 80^\circ$. These deviations from the 90° classical predictions can be attributed the dynamical charges in use which take into account the target nucleus influence on the effective electron–electron interaction.

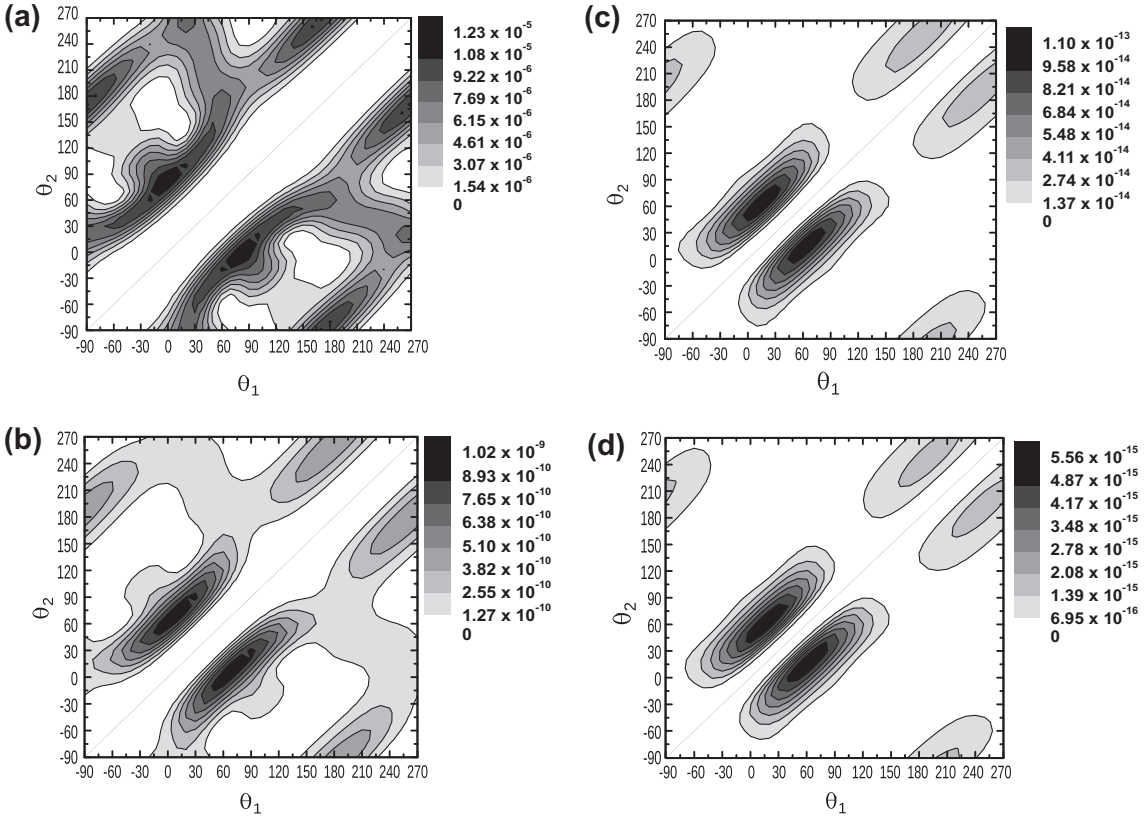

Fig. 3. FDCS scaled in the target nuclear charge for atomic double ionization by proton impact evaluated with the DS3C model. The considered targets are He, Be^{2+}, O^{6+} and Ne^{8+} (a)–(d), respectively. The dynamical quantities for He target are, E_i =700 keV, $E_1 = E_2$ = 10 eV and a fixed projectile scattering angle of $\theta_S = -0.75 \times 10^{-4}$ rad. An energy scaling is applied for the other targets, as described in the text.

For heavier He-like ions, we observe that the structures associated to the mentioned ejection mechanisms evolve in the $\theta_1\theta_2$ plane as $\boldsymbol{Q}$ changes its direction. Due to the increment in the parallel momentum transfer $\Delta E/V$ the $\boldsymbol{Q}$-direction tends to align with the beam direction leading to $\theta_Q = \{71^\circ, 54.5^\circ, 23.3^\circ\}$ for Li^+, Be^{2+}, and B^{3+}, respectively. However, both models present different behaviors. In the 3C model, we observe that the "recoil emission" overcomes the "back-to-back emission" for targets heavier than Be^{2+}. As expected, the inter-electronic repulsion becomes less relevant for larger nuclear charges, as the electron–nucleus interaction increases. In fact, we note that the relative angle θ_{12} for "recoil emission" decreases, and the "back-to-back emission" is reduced. For higher nuclear charges the "binary emission" region appears in the distributions. In the DS3C model, on the other hand, we clearly observe the three structures being the "back-to-back emission" the most important in all cases. This makes sense, since the probability of having a double electronic emission based on separate electron–nucleus target collisions should be larger than an electron–electron collision as the nuclear charge increases. Besides we note that the "recoil emission" gets focused around the classical prediction when the nuclear charge increases. The intensity of the binary emission region slowly increases in comparison with the growth of the recoil lobe. An interesting feature is the split of the binary lobe into two well defined structures in Fig. 2g and h.

We have also carried calculations with the DSC3 method for other electron and projectile energies. As the electrons energies increase from the threshold region, the "back-to-back emission" picture is supressed by the increasing role of the "binary emission" peak and "recoil" peaks. As the target nuclear charge increases, on the other hand, the role of the interelectronic repulsion decreases and the electrons are not forced to escape in a strict collinear geometry [29].

4.2. Energy and momentum scaling laws

From the Schroedinger equation for the present 4-body problem, it is possible to obtain, in the large Z_T limit, a charge independent universal equation in which the projectile and electrons energies scale with the square of the nuclear charge [28,30–32,42]:

$$\frac{E(Z_{T2})}{Z_{T_2}^2} = \frac{E(Z_{T1})}{Z_{T_1}^2} \tag{22}$$

In order to check the most visible differences in the contour plot representation of the FDCS under scaled emission geometries, in Fig. 3 we show FDCS corresponding to 700 keV proton collisions on *He* and $E_1 = E_2 = 10$ eV. The selected targets are He, Be^{2+}, O^{6+} and Ne^{8+} which are shown in Fig. 3a–d, respectively, and for which the scaled energies are $E_0 = 700\ \text{keV}Z_T^2/2^2$ and $E_1 = E_2$=10 eV $Z_T^2/2^2$. These energies corresponds to 2.8 MeV, 11.2 MeV and 17.5 MeV for the impinging projectile and 40 eV, 160 eV and 250 eV for the electrons, respectively. The projectile scattering angle is set at $\theta_S = -0.75 \times 10^{-4}$ rad which corresponds to a momentum transfer value of 0.9 a.u. for He target. From this selection it follows that the momentum transfer scales approximately as the first power of the nuclear charge. We emphasize that the momentum transfer has not a precise scaling, since the ionization energy does not scale as Z_T^2 .

In Fig. 3 we observe that the distributions attain a strong similarity as the nuclear charge increases. We recall at this point that models without angular correlation (Hydrogenic targets plus 2C model) favour the emission of both electrons in the $\boldsymbol{Q}$ direction. It can be seen that as Z_T increases, the distributions tend to the uncorrelated limit and the distributions get localized in the "binary emission" region. However, the Coulomb distortion factor present in the DS3C model prevents the parallel emission keeping a forbidden region

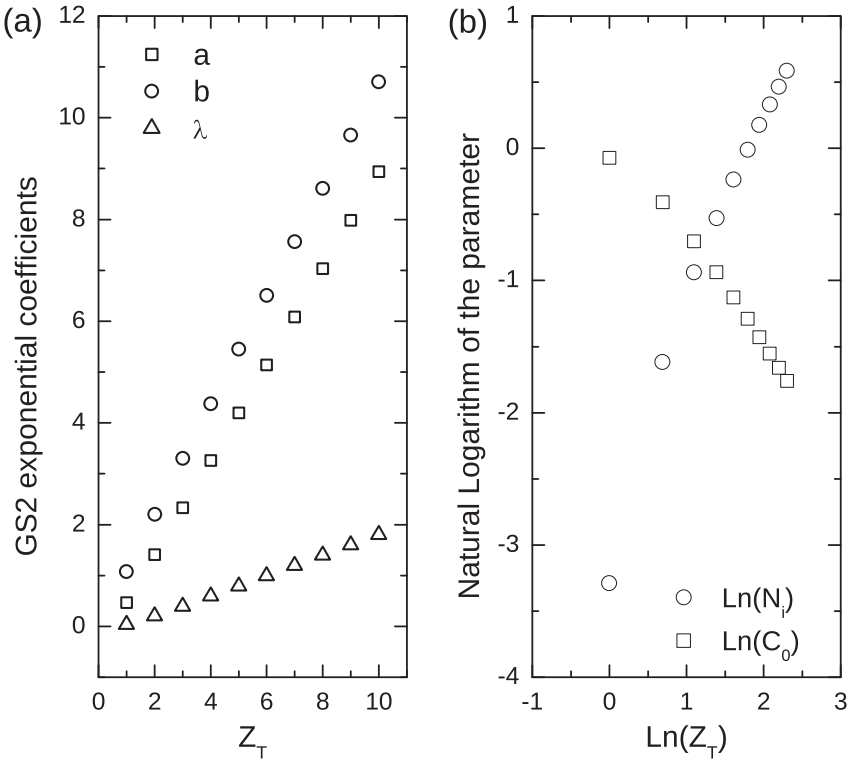

Fig. 4. Variational parameters of the GS2 initial wavefunctions. We display the exponential parameters a (open squares), b (open circles) and λ (open triangles) as a function of the nuclear charge in (a). In (b) we show the natural logarithm of the N_i (open circles) and C_0 (open squares) parameters as a function of the natural logarithm of the nuclear charge.

along the main diagonal. It can be expected that for very asymmetric energy sharing between electrons the scaling of the FDCS converges faster than the symmetric case for large Z_T, and the convergence rate should be determined mainly by the initial state.

We should note that for increasing emission energies, the convergence in shape of the contour plots will be reached faster in Z_T, mainly due to the decreasing relevance of the electron–electron interaction in the collision process.

The remaining point to consider is the possible existence of an overall magnitude scaling for the FDCS as found in photo -double-ionization studies and (e,2e) studies [28–32]. In first place we discuss whether the initial state, the final state and the transition matrix scale with Z_T or not. When the initial and final wavefunctions are uncorrelated, the FDCS in the FBA model present a well defined integer power scaling law. However, this is not the case when initial wavefunctions which explicitly include angular or radial correlation are used. For the GS2 functions, we found that the parameters a, b, and λ behave practically linear with the nuclear charge, although they exhibit different slopes, as can be seen in Fig. 4 a. In Fig. 4b we show the natural logarithm of N_i and C_0 as a function of the natural logarithm of the nuclear charge. The slope of both curves indicates a clear power dependence of $Z_T^{1.15}$ and $Z_T^{-0.92}$ for N_i and C_0, respectively. Thus, it is easy to infer from Eq. (5) that the GS2 functions consist in the sum of two terms with different power laws, one of them corresponding to N_i which scales like $Z_T^{1.15}$ and the other one corresponding to N_iC_0 which scales like $Z_T^{0.23}$. These parameters exhibit an almost linear behavior for large nuclear charges. Therefore the initial state GS2 is a sum of terms with different orders in the Z_T power law. For large Z_T, the term corresponding to N_i dominates and a scaling is recovered for the whole wavefunction. Recall that for the independent electron bound state the normalization factor is proportional to Z_T^3.

On the other hand, the final states hereby considered are angularly correlated. The 3C-type models do not scale with Z_T provided that the interelectronic Sommerfeld parameter does not scale with Z_T . Hence, the explicit inclusion of the interelectronic interaction distorts any possible scaling behavior [32]. As Z_T increases, it is well known that the relevance of the electron–electron interaction decreases in the initial state [28,31,33]. From the analysis we performed above for Fig. 2, we infer that a similar statement applies for the final state.

From the transition matrix Eq. (2) we observe that the initial state introduces a sum of powers of Z_T, and in the FDCS it is unfolded by the squared term. Although the FDCS for He double ionization process have a weak dependence on the initial state electronic correlation [21], it has a relevant role in the FDCS scaling properties. For the independent particle atomic models the scaling law for FDCS in the Eq. (1) is Z_T^{-12} . When we use an uncorrelated final state (2C) and a GS2 initial state the exponent is -15.7, as a consequence of the lower exponent for the normalization [30,32]. We note that for correlated final states, as given by C3 or DS3C wave functions, the asymptotic scaling will depend on the electron emission energies and relative directions [32].

4.3. Influence of the projectile charge sign

In this section we analyze the possible role of the projectile charge sign by means of the DS3C-GO model. Former analyses on this topic were purely experimental and were based on double ionization FDCS for electron and proton impact and were supported by the observation that the ratio between double to single ionization total cross sections has a similar energy dependence for high energies, independently of the projectile mass [15]. However, these are fully integrated cross sections and, in this sense, detailed information on the collision dynamics proper of each projectile is hiddened after the multiple integrations required for that observable.

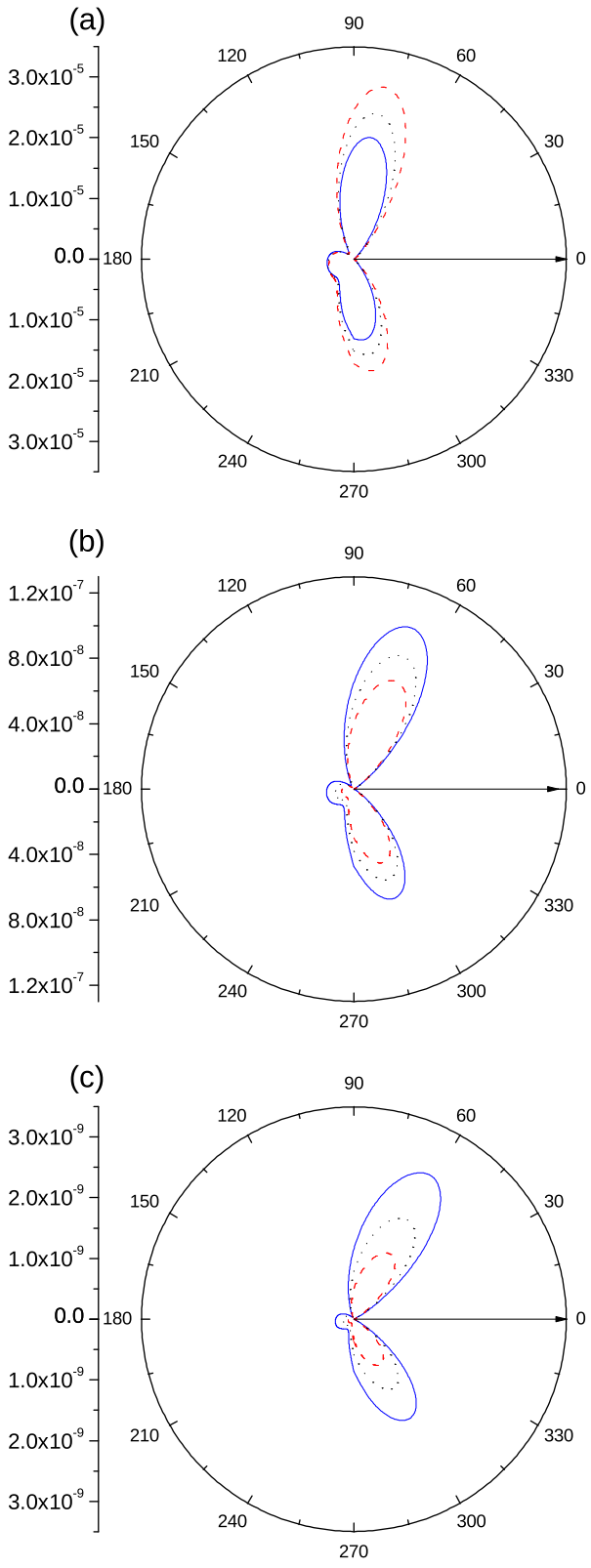

Fig. 5. Polar angle distributions for one electron with the other one emitted in the forward direction (arrow) for double ionization of He, Li^+ and Be^{2+} (a)–(c) by proton (dashed line) and antiproton (full line) impact. These FDCS are obtained with the DS3C-GO model. The incident projectile energy considered for helium target is $E_i = 1$ MeV, the electron energies: $E_1 = E_2 = 10$ eV. For the other targets we applied the proposed scaling $E_0 = (Z_T/2)^2$ MeV and $E_1 = E_2 = 10\ (Z_T/2)^2$ eV. The projectile scattering angle is fixed at $\theta_S = -1 \times 10^{-5}$ rad. The results obtained by means of the DS3C model are shown with dotted-lines.

In Fig. 5 we consider proton and antiproton collisions on He (a), Li^+ (b) and Be^{2+} (c), under a fixed scattering angle of 1×10^{-5} rad . For He target the projectile impact energy considered is 1 MeV/amu and the electrons energies are of 10 eV each. For the other targets under consideration, these energies are scaled as in the previous section. For the three cases, the momentum transfer direction is approximately at 9° from the beam direction, and its magnitude increases as the first power of Z_T . In the present polar representation, one electron is fixed at the forward direction, here indicated by an arrow, with the FDCS given in terms of the angular distribution of the other electron. To complete our description, results obtained with the DS3C model are also displayed. Their inclusion helps to visualize the influence of the projectile charge sign in the electronic emission spectra.

For He target, we note that the FDCS for proton impact present higher values than those corresponding to antiproton impact. This behavior reverses for increasing target nuclear charges as can be seen from the present results for Li^+ and Be^{2+}. These differences between proton and antiproton impact are produced by the antiproton pushing the electrons into the atom favouring those structures that involve the collision of the electrons with the target [21].

To summarize, it is in the combined effect of the growth of Z_T and the effect of the proton (antiproton) on the electrons trying to pull (push) them from (on) the nuclear charge that we find the reason why for Li^+ and Be^{2+} the antiproton impact FDCS are larger than the proton impact case. Another important feature is the reduction of the interelectronic angle as Z_T increases. This clear footprint of the weakening of the interelectronic repulsion, is found in our distributions irrespective of the projectile charge sign under consideration.

5. Conclusions

In this work we have theoretically studied the double ionization of the He-isoelectronic series by means of a recently introduced distorted wave model based on dynamical effective charges. The present analysis has been restricted to two electrons emitted with equal energies.

Three main collision mechanisms for the double electronic emission were identified and associated to different regions of the momentum distribution. These were denoted as: back-to-back emission, recoil emission and binary emission and provide classical pictures of the double emission which can be easily recalled when analyzing the contour plot representation of the FDCS. The influence of the nuclear target charge at the fully differential level has been analyzed in terms of these collision mechanisms.

As expected, we have found that the increase of the target nuclear charge leads to an enhancement of the structures which involve collisions between the electrons with the target nucleus. In this sense, the study of the He-isoelectronic sequence leads to a more general understanding of the role the recoiling target ion plays on the two-electron emission dynamics.

Besides, we note that the decreasing role of the interelectronic repulsion as Z_T increases has a noticeable effect in the "binary emission" and the "recoil emission" (mechanisms which involve an electron–electron collision) leading to interelectronic emission angles which get closer to the orthogonal classical prediction.

FDCS for scaled momenta and impact energies have been shown to provide insight on the relative contributions of the acting interactions at equivalent emission geometries. The scaling properties of the initial and final wavefunctions have been analyzed and the difficulties associated to the determination of a universal scaling law for the FDCS have been discussed.

Finally, we explored the possible influence of the projectile charge sign at the fully differential level. We observed that for intermediate impact energy the projectile charge sign plays a role, as expected [21]. We note that the differences between proton and antiproton impact are more noticeable as the nuclear target charge increases.

Provided the experimental advance in the field that we have witnessed in the last few years, a more exhaustive analysis of proton impact double ionization processes on atomic targets seems imperative and would be welcome to further test and refine the present theoretical models.

Acknowledgments

This work was supported by PGI 24/F049 of UNS, PICT 2007-00887 of ANPCyT and PIP 112-200801-02760 of CONICET (Argentina).

References

[1] T.E. Cravens, Science 296 (2002) 1042.
[2] S. Otranto, R.E. Olson, P. Beiersdorfer, J. Phys. B: At. Mol. Opt. Phys. 40 (2007) 1755.
[3] S. Otranto, R.E. Olson, Phys. Rev. A 83 (2011) 032710.
[4] B. Gervais, M. Beuve, G.H. Olivera, M.E. Galassi, Radiat. Phys. Chem. 75 (2006) 493.
[5] M.B. Shah, H.B. Gilbody, J. Phys. B: At. Mol. Opt. Phys. 18 (1985) 899.
[6] L.H. Andersen et al., Phys. Rev. Lett. 57 (1986) 2147.
[7] J.H. McGuire, L. Weaver, Phys. Rev. A 16 (1977) 41.
[8] N.C. Deb, D.S.F. Crothers, J. Phys. B: At. Mol. Opt. Phys. 24 (1991) 2359.
[9] M. McCartney, Nucl. Instrum. Methods Phys. Res. B 155 (1999) 343.
[10] J. Bradley, R.J.S. Lee, M. McCartney, D.S.F. Crothers, J. Phys. B: At. Mol. Opt. Phys. 37 (2004) 3723.
[11] M. Fiori, A.B. Rocha, C.E. Bielschowsky, G. Jalbert, C.R. Garibotti, J. Phys. B: At. Mol. Opt. Phys. 39 (2006) 1751.
[12] L. Gulyás, A. Igarashi, P.D. Fainstein, T. Kirchner, J. Phys. B: At. Mol. Opt. Phys. 41 (2008) 025202.
[13] J.F. Reading, A.L. Ford, Phys. Rev. Lett. 58 (1987) 543.
[14] R.E. Olson, Phys. Rev. A 36 (1987) 1519.
[15] D. Fischer et al., Phys. Rev. Lett. 90 (2003) 243201.
[16] D. Fischer, M. Schulz, R. Moshammer, J. Ullrich, J. Phys. B: At. Mol. Opt. Phys. 37 (2004) 1103.
[17] M.F. Ciappina, M. Schulz, T. Kirchner, D. Fischer, R. Moshammer, J. Ullrich, Phys. Rev. A 77 (2008) 062706.
[18] E.M. Lobanova, S.A. Sheinerman, L.G. Gerchikov, J. Expt, Theor. Phys. 105 (2007) 486.
[19] M. Foster, J. Colgan, M.S. Pindzola, J. Phys. B: At. Mol. Opt. Phys. 41 (2008) 111002.
[20] X. Guan, K. Bartschat, Phys. Rev. Lett. 103 (2009) 213201.
[21] S.D. López, C.R. Garibotti, S. Otranto, Phys. Rev. A 83 (2011) 062702.
[22] S.J. Ward, J.H. Macek, Phys. Rev. A 49 (1994) 1049.
[23] S. Otranto, G. Gasaneo, C.R. Garibotti, Nucl. Instrum. Methods Phys. Res. B 217 (2004) 12.
[24] C.R. Garibotti, J.E. Miraglia, Phys. Rev. A 21 (1980) 572.
[25] M. Brauner, J.S. Briggs, H. Klar, J. Phys. B: At. Mol. Opt. Phys. 22 (1989) 2265.
[26] J. Berakdar, J.S. Briggs, Phys. Rev. Lett. 72 (1994) 3799.
[27] J. Berakdar, Phys. Rev. A 53 (1996) 2314; 54 (1996) 1480.
[28] M.A. Kornberg, J.E. Miraglia, Phys. Rev. A 49 (1994) 5120.
[29] S. Otranto, C.R. Garibotti, Eur. Phys. J. D 27 (2003) 215.
[30] C.R. Stia, O.A. Fojón, R.D. Rivarola, J. Phys. B: At. Mol. Opt. Phys. 33 (2000) 1211.
[31] A.L. Frapiccini, K.V. Rodriguez, G. Gasaneo, S. Otranto, Braz. J. Phys. 37 (2007) 1115.
[32] M.K. Srivastava, PRAMANA J. Phys. 63 (2004) 1053.
[33] L.U. Ancarani, C. Dal Cappello, I. Charpentier, K.V. Rodriguez, G. Gasaneo, Phys. Rev. A 78 (2008) 062709.
[34] G. Gasaneo, S. Otranto, K.V. Rodriguez, Proc. XXIV Int. Conf. Photonic, Electronic and Atomic Collisions, World Scientific, Singapore, 2006, p. 360.
[35] S. Jetzke, S.H.M. Faisal, J. Phys. B: At. Mol. Opt. Phys. 25 (1992) 1543.
[36] S. Otranto, C.R. Garibotti, Eur. Phys. J. D 21 (2002) 285.
[37] J.R. Götz, M. Walter, J.S. Briggs, J. Phys. B: At. Mol. Opt. Phys. 39 (1999) 4532.
[38] A. Dorn, A. Kheifets, C.D. Schröter, B. Najjari, C. Höhr, R. Moshammer, J. Ullrich, Phys. Rev. Lett. 86 (2001) 3755.
[39] A. Lahmam-Bennani, E.M. Staicu-Casagrande, A. Naja, C. Dal Cappello, P. Bolognesi, J. Phys. B: At. Mol. Opt. Phys. 43 (2010) 105201.
[40] S. Otranto, R.E. Olson, J. Fiol, J. Phys. B: At. Mol. Opt. Phys. 39 (2006) L175.
[41] M.A. Kornberg, J.E. Miraglia, Phys. Rev. A 48 (1993) 3714.
[42] S. Otranto, C.R. Garibotti, Eur. Phys. J. D 27 (2003) 215.